Published in final edited form as:
Curr Pharm Des. 2013 ; 19(37): 6594–6605.

Design and *In vitro* Validation of Multivalent Dendrimer Methotrexates as a Folate-targeting Anticancer Therapeutic

Thommey P. Thomas[1,2,*], **Melvin Joice**[1,2], **Madhuresh Sumit**[3], **Justin E. Silpe**[2,4], **Alina Kotlyar**[1,2], **Sophia Bharathi**[1,2], **Jolanta Kukowska-Latallo**[1,2], **James R. Baker Jr.**[1,2], and **Seok Ki Choi**[1,2,*]

[1]Department of Internal Medicine, University of Michigan, Ann Arbor, MI 48109, USA

[2]Michigan Nanotechnology Institute for Medicine and Biological Sciences, University of Michigan, Ann Arbor, MI 48109, USA

[3]Program in Biomedical Science, University of Michigan, Ann Arbor, MI 48109, USA

[4]Department of Macromolecular Science and Engineering, University of Michigan, Ann Arbor, MI 48109, USA

Abstract

Design of cancer-targeting nanotherapeutics relies on a pair of two functionally orthogonal molecules, one serving as a cancer cell-specific targeting ligand, and the other as a therapeutic cytotoxic agent. The present study investigates the validity of an alternative simplified strategy where a dual-acting molecule which bears both targeting and cytotoxic activity is conjugated to the nanoparticle as cancer-targeting nanotherapeutics. Herein we demonstrate that methotrexate is applicable for this dual-acting strategy due to its reasonable affinity to folic acid receptor (FAR) as a tumor biomarker, and cytotoxic inhibitory activity of cytosolic dihydrofolate reductase. This article describes design of new methotrexate-conjugated poly(amidoamine) (PAMAM) dendrimers, each carrying multiple copies of methotrexate attached through a stable amide linker. We evaluated their dual biological activities by performing surface plasmon resonance spectroscopy, a cell-free enzyme assay and cell-based experiments in FAR-overexpressing cells. This study identifies the combination of an optimal linker framework and multivalency as the two key design elements that contribute to achieving potent dual activity.

Keywords

Folate Receptor; Methotrexate; Dihydrofolate Reductase; PAMAM Dendrimer; Multivalent Binding; Drug Delivery

Introduction

Targeted delivery based on multifunctional nanoparticles (NPs) has continued to make significant contributions in the discovery of novel diagnostic tools and effective therapeutics applicable for several critical disease areas including cancers and inflammatory diseases [1–8]. However the development of such multifunctional NPs faces several challenging issues that are attributable primarily to the structural complexity associated with the NP design such as targeting ligand density, drug payloads, and distribution of the NP size [9–13]. This

*To whom correspondence should be addressed, Phone: (734) 615-0618; Fax: (734) 615-0621; skchoi@umich.edu, Phone: (734) 647-2777; Fax: (734) 615-2506; thommey@umich.edu..

study aims to validate a simplified strategy for identifying cancer-targeted therapeutics in a design that involves functionalization of a NP with a dual-acting molecule, in lieu of two single-acting molecules, that serves as *both* a targeting ligand and a cytotoxic agent (Figure 1). We believe that this dual-acting molecular strategy can be more effective for the control of NP distribution and property than a conventional approach which otherwise relies on the co-functionalization with two distinct single-acting molecules.

Multifunctional NPs have been extensively investigated for cancer-targeted therapeutic delivery by targeting a range of tumor biomarkers that include folic acid receptor (FAR) [3, 14–17], $\alpha_v\beta_3$ integrin [18–22], prostate-specific membrane antigen [23–24], riboflavin receptor [5, 25–26], and epidermal growth factor receptor [6, 27–28]. In this delivery strategy, each NP was functionalized by presenting a specific ligand molecule that binds such a tumor biomarker, as well as by carrying multiple copies of a cytotoxic therapeutic agent. Here, we evaluate our new design strategy by focusing on the FAR which is frequently overexpressed on the surface of epithelial cells in breast, and ovarian cancers [29]. As a membrane-bound receptor, FAR recognizes folic acid (FA) with a nanomolar affinity (K_D = 0.4 nM) [30], and uptakes the FA ligand or its conjugate into the cytosol through FAR-mediated endocytosis [2]. Thus FAR provides unique opportunities for tumor-specific binding and cellular entry of those chemotherapeutics and imaging molecules conjugated with the FA or to the FA-presenting NP (Figure 1) [1–2, 29, 31]. In search for a small dual-acting molecule that displays the targeting activity for FAR, we have been interested in methotrexate (MTX, Figure 2). As one of the antifolate molecules, MTX has been used as an anticancer drug [3, 32]. Its therapeutic efficacy is attributed to its potent activity to inhibit several metabolic enzymes including primarily dihydrofolate reductase (DHFR; K_i = 1.2 nM), a cytosolic enzyme responsible for purine and thymidylate biosynthesis (Table 1) [33]. In addition, its high structural homology to FA (Figure 2) confers the ability to bind FAR though at a reduced affinity (K_D = ~20–100 nM) [30, 34–35]. Otherwise both FA and MTX display similar physico-chemical properties as summarized in Table 1. Like FA, MTX displays a hydrophilic property (negative logD, large tPSA), in large part, due to its two carboxylic acids that are ionized at physiological pH (pK_a = 3.8, 4.8). Because of such properties, MTX is unable to cross the cell membrane passively (low Caco2 value [36]) unless uptaken in an active mechanism mediated by cell surface proteins like FAR and reduced folate carrier [37].

Thus MTX provides both cytotoxicity and FAR targeting capability, the dual activity required in the current delivery strategy. However MTX has a suboptimal affinity to FAR, and may be intrinsically less efficient for FAR targeting than FA. Despite its lower FAR affinity, we hypothesize that its targeting capability can be enhanced through the concept of multivalent ligand design as applied in this study (Figure 1) [38–41]. Compared to a monovalent ligand, the multivalent ligand is characterized to bind simultaneously to multiple receptors on the surface, and displays collectively much tighter association (avidity) than the affinity displayed by each individual ligand attached [39]. Recently, we investigated such multivalent interactions by surface plasmon resonance (SPR) spectroscopy for multivalent dendrimer NPs, each presenting multiple FA [42] or MTX [43–44] molecules conjugated to a fifth generation (G5) poly(amidoamine) (PAMAM) dendrimer scaffold. These SPR studies demonstrated that the FA-or MTX-presenting multivalent conjugate binds to folate binding protein (FBP) immobilized on the surface by three to five orders of magnitude more tightly than free FA or MTX. Such notable multivalent effects support that MTX could serve as an effective dual-acting agent for cancer-targeted therapeutic and diagnostic applications.

Recently, we reported the synthesis of G5-MTX_n conjugate, each MTX tethered through a cyclooctyne-based linker by copper-free click chemistry [45]. We demonstrated that this

G5-MTX_n conjugate was stable in serum and able to undergo internalization into FAR-expressing cells to induce cytotoxicity [44]. In the present study, we were interested in further defining the design aspects of the dendrimer-based multivalent MTX NP as an approach to better understand the correlation between its linker length and dual activity. Thus instead of using the cyclooctyne-based linker that provides a fixed length, we introduced a new amide-based, oligo(ethyleneglycol) spacer that allows to vary the linker length through a repeated elongation of its ethyleneglycol units. In addition, the linker chemistry we used allows easier scale up as compared to the cyclooctyne-based strategy. The present study investigates structural-activity correlation of the linker length, and provides evidence that the avidity of the MTX conjugate is determined primarily by multivalent effect independent of the linker structure while its cytotoxicity is highly dependent on the linker length.

Results and Discussion

Design of G5 PAMAM dendrimer conjugated with MTX through an extended linker

Our earlier study [43] reported the design of G5 PAMAM dendrimer conjugated with a variable number of MTX molecules attached on the neutral surface of the dendrimer as represented by **1** Ac-G5-MTX_n (n = mean valency = 5) in Figure 3. In that series, each MTX is tethered through an amide bond formed without any intervening spacer between the carboxylic acid of the MTX (L)-glutamate and the primary amine located on the dendrimer periphery. The SPR study performed for such no spacer series demonstrated enhancement of their binding avidity to the folate receptor on the surface by 10^3 to 10^4-fold over free MTX as illustrated by **1** ($K_D = 2.6\times10^{-8}$ M). Such remarkable multivalent effect [43] is also consistent with the FAR-mediated cellular uptake of MTX-conjugated dendrimers in a KB cancer cell which over-expresses a high level of FAR [42]. Despite such FAR-mediated targeting, the no-spacer MTX conjugates were minimally active in inhibiting growth of KB cells at up to low μM concentrations (<10% inhibition, see below).

We hypothesized that such weak cytotoxicity might be attributable to the amide linkage used in the MTX conjugation. This amide linkage was selected because of its potential ability to provide greater conjugate stability and longer duration in the plasma than the common ester-based linkage which is easily hydrolysable chemically or enzymatically. But it might be too stable for releasing a cytotoxic level of free MTX, or too short in the linker length for inducing enzyme inhibition otherwise by a still tethered MTX molecule. In particular, the MTX conjugated without any spacer is located in a sterically congested environment because of its close proximity to the dendrimer periphery [43], and thus it might be unable to get easy access to the catalytic site of DHFR as its target enzyme (cf. the crystal structure of human DHFR [46] inhibited by a free methotrexate molecule in Figure 1) [27, 47].

In an approach to address the issue of MTX attachment, we redesigned the amide linker framework primarily by extending its length (Figure 3). In this linker design, we introduced two types of spacers (S1 and S2), each based on a non-rigid ethyleneglycol (EG) linear chain but different in the length. As summarized in Table 2, Table S1 consists of a 15-atom spacer (length ≈ 22 Å at a fully extended conformation), but is 2-fold shorter than S2 composed of two repeating S1 units (extended length ≈ 44 Å). These EG-based spacers are largely hydrophilic as predicted by their values of negative logP and large tPSA. Thus, each MTX molecule tethered by such extended linker is expected to be more flexible in its molecular motion, more exposed to water, and better able to inhibit the DHFR enzyme.

Synthesis of G5-MTX conjugates

Scheme 1 describes synthesis of G5 PAMAM dendrimers **2–4**, each presenting MTX molecules attached through the extended spacer 1 or 2. First, G5 PAMAM dendrimer G5-NH_2 (mean number of primary amines = 114) was fully derivatized with glutaric anhydride to prepare glutaric acid (GA)-terminated dendrimer **5** G5-GA (M_n = 42730 $gmol^{-1}$, PDI = M_w/M_n ~1.046) as described elsewhere [48–50]. Each GA branch was further modified to extend the spacer length by covalent coupling with $H_2N(CH_2CH_2O)_2CH_2CH_2NH$-GA through an amide linkage which led to **6** G5-EG-GA. This modified dendrimer was fully characterized by a number of standard analytical methods including gel permeation chromatography (GPC) (M_w = 81450 $gmol^{-1}$; M_n = 70000 $gmol^{-1}$; PDI = 1.163), ^1H NMR spectroscopy [51–52], and ultra performance liquid chromatography (UPLC) as illustrated in Figure 4. In a next step for MTX conjugation with the surface-modified dendrimer **5** and **6**, MTX was preactivated by treatment with PyBOP and HOBT reagents, and subsequently reacted with one molar equivalent of $H_2N(CH_2CH_2O)_2CH_2CH_2NH_2$ in a one-pot reaction process, yielding **7** MTX-$C(=O)NHCH_2CH_2(OCH_2CH_2)_2NH_2$ as a desired monoadduct. This reaction also generated a diadduct, but due to lack of a terminal amino group, this undesired product is able to react with the activated ester in the dendrimer conjugation step. The amine-terminated MTX derivative **7** was then covalently attached to either dendrimer **5** or **6** by a method that involves preactivation of the carboxylic acid terminated on the dendrimer surface to its *N*-hydroxysuccinimide. This sequential one-pot method allowed the rapid synthesis of the conjugates **2–4**. The number of MTX attached to each dendrimer was controlled by varying the molar ratio of **7** to the carboxylic acid residues of the dendrimer. Each of the resultant dendrimer conjugates was purified by dialysis using a membrane tubing (MWCO 10 kDa), and fully characterized by analytical methods including ^1H NMR spectroscopy [51], UV-vis spectrometry [43], and analytical UPLC (purity ≥98%) (Figure 4). The number (n) of MTX tethered per dendrimer nanoparticle was determined on a mean basis by the NMR integration method as its details are described in the experimental section [43, 49–50].

Surface plasmon resonance (SPR) spectroscopy

We performed SPR experiments for investigating the multivalent interaction of the MTX conjugate with folate binding protein (FBP) by selecting the conjugate **4** G5-(S2)-MTX_{12} as a representative conjugate. As a bioanalytical method well established for studying interactions on biological surfaces on a real time basis, SPR spectroscopy is highly suitable for the studies involving multivalent ligand-receptor interactions in targeted delivery [42–44]. First, we immobilized FBP (bovine milk) as a model protein for the membrane-bound FAR on the surface of a CM5 sensor chip following an EDC/NHS method as described [42]. This process led to the FBP immobilization at the surface density of 11 ng FBP/mm^2 (3.7×10^{-13} mol/mm^2). Then we performed the binding studies of monovalent control ligands (FA, MTX) as illustrated by their select SPR sensorgrams in Figure 5. Given the monovalent mode of receptor-ligand association, each sensorgram was analyzed by a curve fitting based on 1:1 Langmuir model [42], and the equilibrium dissociation constants were determined ($K_D = k_{off} \div k_{on}$) as summarized in Table 3. The results suggest that MTX binds to the FBP with a K_D value of 1.7×10^{-5} M, an affinity ~5-fold lower than that of FA ($K_D = 3.5 \times 10^{-6}$ M in this study; 5×10^{-6} M [42]).

Finally, we studied the binding kinetics of conjugate **4** by acquiring a series of SPR sensorgrams generated in a concentration-dependent manner (Figure 5c). Its sensorgams indicate that the conjugate binds to the surface even at low μM concentrations, which is highly notable because such binding activity could not be achieved by FA or MTX at the same condition. A fully acetylated neutral dendrimer Ac-G5 was tested as a negative control dendrimer because of its lack of conjugation with either MTX or FA (Figure 5d). Its

injections which were made otherwise under comparable concentrations to **4** did not show any meaningful level of dendrimer adsorption to the FBP surface, confirming the specificity of the FBP surface. Each sensorgram acquired by **4** is characterized by slow dissociation which is in contrast to the rapid dissociation displayed by FA and MTX. This kinetic feature is consistent with those observations made in numerous other multivalent systems [42–44, 53–55], including the reference conjugate **1** Ac-G5-MTX_5 we reported earlier[42]. The dissociation phase of **4** suggests that it dissociates apparently in multiple phases, initially a rapid off rate, and subsequently slower off rates. For example, ~23(±10)% of fractional desorption (= $RU_D/RU_A \times 100(\%)$) was observed per initial 5s followed by 56(±8)% of fractional desorption observed at the end of data collection time when the dissociation appears still incomplete. Such mixed dissociations displayed by **4** might reflect, in part, the preexisting distribution of the conjugate population with regards to MTX valency. While the MTX valency of **4** G5-(S2)-MTX_{12} is assigned as 12 which is calculated on an average basis, our recent studies suggest that it is composed of wide distribution of multivalent dendrimer species (n = 8–15 making nearly 80% of total population) when simulated according to Poissonian distribution [9, 56].

In order to determine the dissociation constant K_D of **4**, we analyzed the SPR data on a quantitative basis by using non-linear regression method as already established for the SPR analysis [57]. This method enabled us to extract the estimates for its kinetic rate constants (k_{on}, k_{off}) and the K_D value as summarized in Table 3. The K_D value (18 nM) of **4** suggests that its binding avidity is enhanced by a factor of 944 (multivalent binding enhancement = β) relative to free MTX molecule (K_D = 17 μM). This conjugate is comparable to the other conjugate **1** **Ac**-G5-MTX_5 which shows the K_D value of 26 nM with the β value of 923. So, the spacer appears to make almost no effect on the dissociation constants in the model surface. The primary kinetic parameter that accounts for avidity enhancement for **4** is attributable to its slower off rate ($k_{off} = 5.9 \times 10^{-4}\ s^{-1}$). As already discussed earlier by fractional desorption, this dissociation feature is in full agreement with other reports that complete dissociation by a multivalent conjugate occurs very slowly because it requires simultaneous dissociation of all the ligands tethered to a single multivalent species from multiple receptor sites [39, 54–55]. In summary, the present SPR study demonstrated that the multivalent PAMAM dendrimer conjugated with MTX through an extended spacer binds to the surface FBP by almost three orders of magnitude more tightly than a free MTX molecule. It supports the validity of our strategy to target FAR-overexpressing cancer cells by using MTX-presenting multivalent dendrimers.

Dihydrofolate reductase (DHFR) assay

Based on the SPR study presented in Figure 5 and our previous studies showing the high-avidity binding of S0-linked MTX-conjugates [43], the length of a MTX spacer to the dendrimer does not serve the primary factor that determines binding avidity to the FAR model surface. We were interested in investigating the effect of the spacer length on other functional activity by MTX. While detailed studies are needed to understand the rate of internalization, intracellular localization, as well as the mechanisms of action of the MTX conjugates after cellular entry, we focused on a cell-free enzyme assay using human DHFR, the primary cytosolic enzyme targeted by MTX [15, 43]. It is important to note that this assay was performed in a PBS solution only for a short period of time (≤ 5 min) in which the amide linkage should remain completely stable with the MTX molecule still tethered to the dendrimer [43]. The DHFR assay [15, 43] showed that both **4** G5-(S2)-MTX_{12} and **3** G5-(S2)-MTX_4, each conjugated through the longer spacer S2 but with different MTX attached, inhibited the enzyme activity, though less potently than free MTX (Figure 6). In contrast, other two conjugates **1** G5-(S0)-MTX_5 and **2** G5-(S1)-MTX_3 where each MTX is conjugated with either a no spacer or shorter spacer, showed only weak or no inhibitory

activity. The assay results suggest the existence of certain threshold in the spacer length for the tethered MTX to bind into the catalytic pocket of DHFR (Figure 2b). The reason for the observed higher DHFR inhibition by **3** G5-(S2)-MTX_4 as compared to the **4** G5-(S2)-MTX_{12} (Figure 6) is not known. It is possible that as only one MTX moiety on the dendrimer can bind to the DHFR active site, the higher surface density of MTX in the G5-(S2)-MTX_{12} may result in mutual steric hindrance for active site occupation. The results of the DHFR study emphasize that the spacer length is an important design factor that can determine the functional activity associated with tethered MTX. Moreover, although increased MTX surface density may facilitate FAR binding, it appears that DHFR inhibition is more favored at lower MTX surface density (<4 per dendrimer). Although these S2-linked conjugates showed significantly lower DHFR inhibition than free MTX, the conjugates may induce a still sufficient level of cytotoxicity because of the 10^3- to 10^4-fold higher affinity of MTX than folate for DHFR [58].

In summary, the DHFR enzyme assay shows potent inhibitory activity by the conjugates in which the MTX was linked through the long S2 linker. This DHFR assay provided us with a piece of information to understand the mode(s) of action by the S2-linked conjugates. However such simple mode of action could become more complex *in vitro* and *in vivo* than the cell-free condition. For example, it is possible that a fraction of MTX is released from the conjugate in circulation and in cytosolic compartments because its amide linkage is slowly cleavable by esterases and proteases in these milieu, and by low pH [59].

In vitro cell-based binding

After multivalent tight binding by MTX conjugate **4** was observed in the SPR study, we were interested in determining if its high avidity can be translated to its FAR-targeting ability on the cell surface. We utilized two fluorescently-labeled dendrimer conjugates 'G5-(S2)-MTX_{12}-AF_3' and 'G5-(S2)-MTX_4-FI_2' in which each fluorescent dye Alexa Fluor 488 (AF) or fluorescein isothiocytanate (FITC, FI) was covalently linked as described in Methods. For these binding studies, we used 3 different cell lines, the KB epithelial and RAW264.7 macrophage cell lines which express high FAR and the B16-F10 melanoma cell line which express low FAR [4, 44]. As shown in Figure 7, each of the conjugates bound to the FAR-expressing KB and RAW264.7 cells in a dose-dependent manner, whereas in the low-FAR B16-F10 cells, it showed ~5-fold lower maximal binding at 300 nM. Control conjugates that lack the MTX moiety failed to bind to the FAR-expressing KB cells, and the binding was inhibited by pre-incubation with 50-fold excess free FA (Figure 8). In summary we observed significantly reduced binding in FAR-negative B16-F10 cells relative to the FAR-positive cells, the failure of binding of the MTX-lacking control conjugates, and the reversal of binding of the MTX conjugates by free FA. All of these results suggest that the G5-(S2)-MTX_{12} conjugates bind to the cells specifically through the interaction of the MTX with FAR on the cell surface.

Cytotoxicity

We then tested the cytotoxicity of all MTX conjugates linked through the three different linkers S0, S1 and S2 by an XTT assay. As shown in Figure 9, **4** G5-(S2)-MTX_{12} induced a dose-dependent cytotoxicity whereas the S0- and S1-linked conjugates **1** and **2** failed to induce any significant cytotoxicity whether the dose was expressed on either conjugate (Figure 9A) or MTX (Figure 9B) concentrations. Negative controls—those dendrimers without MTX conjugated [5, 31, 44]—did not show any cytotoxicity to KB cells when tested under an identical assay condition (not shown). These include acetylated PAMAM dendrimers [31], **5** G5-GA [5] and other dendrimers conjugated with FA or nontoxic small molecules alone [5, 31, 44]. The absence of any cellular activity of the surface-neutralized dendrimer platform is also evident from the observations that the control dendrimers G5-AF

and G5-FI failed to bind to KB cells (Figure 8) and the S0- and S1-linked conjugates failed to show any cytotoxicity (Figure 9). However, evaluating the inhibitory capacity based on MTX-concentration may be less relevant due to the expected stability of the amide linked MTX and the possible lack of DHFR active site binding by all MTX presented by a dendrimer molecule. In this experiment, we also tested the cytotoxicity of G5-(S2)-FI-MTX_4, which showed a modest induction of cytotoxicity. The reduced cytotoxic potential of the G5-(S2)-FI-MTX_4 compared to G5-(S2)-MTX_{12} is possibly due to its lower avidity in the FAR binding, as we have observed previously [44].

As presented here, free MTX shows activities *in vitro* more potent than its dendrimer conjugates in the DHFR inhibition assay (Figure 6) and the cytotoxicity assay (Figure 9). Despite the fact that free MTX has a lower affinity for FAR than the multivalent G5-(S2)-MTX_{12} (Figure 5), MTX can enter cells also through the reduced folate carrier (RFC) [60], ubiquitously present in all cell types, and perhaps via some passive diffusion across the membrane. However, the larger dendrimer conjugates are not internalized into the cells through either of these pathways [44], thus providing specificity of the conjugate for cells which express FAR, as demonstrated in Figure 7. Therefore, despite the observed higher DHFR inhibition and *in vitro* cytotoxicity of free MTX, we expect that its conjugate will have higher efficacy *in vivo* for targeting and killing FAR-expressing cancer cells than normal healthy cells. Moreover, the increase in *in vivo* efficacy of the conjugate will be further complemented by its longer blood half-life as compared to MTX [1]. We believe that the combination of the high avidity multivalent binding, tumor specificity and extended duration of circulation will make the G5-(S2)-MTX_{12} a preferred cancer nanotherapeutic agent over free MTX.

In summary, the cell-based studies provide evidence that the MTX molecule tethered to a dendrimer through the S2 linker plays a dual role: i) the targeting ligand that enables binding and uptake by a FAR-overexpressing cell; ii) the therapeutic agent that inhibits cell growth. Level of such dual activity could be tunable in principle by the combination of such design factors as MTX valency, and spacer length.

Conclusion

The present study describes and validates the new proof of concept strategy for cancer-targeted delivery. As a dual-acting therapeutic agent, MTX was conjugated to a fifth generation PAMAM dendrimer as the multivalent scaffold carrier. Each MTX was attached to the terminal branch of the dendrimer through an EG-based extended spacer which was developed to provide stability and to optimize the enzyme inhibitory activity. Our SPR and cell-based experiments suggest that the multivalent MTX conjugate targets FARs via multivalent binding effect by the FAR-overexpressing cell, and subsequently inhibits the cell growth after cellular internalization. These results also suggest that a tether length of <2.2 nm (spacer 1 at a fully extended conformation; Table 2) between the MTX and dendrimer might be insufficient for DHFR binding and induction of cytotoxicity, but a length of 4.4 nm (spacer 2) could be sufficient. We believe that this FAR-targeted dual-acting strategy is potentially applicable in a similar design for other MTX-like antifolate drug molecules[61] by replacing MTX with the antifolate like pemetrexed and raltitrexed as the dual-acting agent. The synthetic strategy described here is designed to allow easier scale up as compared to the cyclooctyne- and click chemistry-based multivalent G5-MTX_n conjugates we developed recently [44]. This advantage is a crucial determining factor for development of this nanotherapeutic for clinical applications. Future efforts will focus on enhancing the scope and *in vivo* applications of this strategy in cancer and other related diseases.

Materials and Methods

Materials

All solvents and reagents were purchased from commercial suppliers, and used without further purification unless specified. Such materials and reagents include folate binding protein (bovine milk; Sigma-Aldrich), methotrexate hydrate (TCI; purity >98.0%), fluorescein 5(6)-isothiocyanate (Sigma-Aldrich; purity ~90%), 1-ethyl-3-(3-dimethylaminopropyl) carbodiimide hydrochloride (EDC; Sigma-Aldrich), benzotriazol-1-yloxy-tripyrrolidino-phosphonium hexafluorophosphate (PyBOP; Bachem), and Alexa Fluor 488 hydrazide (Molecular Probes®). Generation 5 (G5) poly(amidoamine) (PAMAM) dendrimer was purchased as a 17.5 % (wt/wt) methanol solution (Dendritech, Inc., Midland, MI), and was purified by dialysis prior to use as described elsewhere (M_w = 26550 $gmol^{-1}$; M_n = 26270 $gmol^{-1}$; polydispersity index, PDI = 1.010) [51]. The average number of primary amines per dendrimer particle was determined by the potentiometric titration method as reported earlier [10, 51]. The number of primary amines determined for this G5 dendrimer was 114 on a mean basis. G5 dendrimer modified with glutaric acid G5-GA **5** [48], and the dendrimer conjugated with MTX through the S0 linker G5-(S0)-MTX_5 **1** [43] were prepared as described elsewhere. **1**: UPLC analysis: t_r = 8.21 min; purity: 99 %. UV/vis (PBS, pH 7.4): 380, 310, 263 nm.

Methods

Characterization of G5 PAMAM dendrimer and its conjugates was carried out by standard analytical methods as described earlier [5, 25, 48–51]. ^{1}H NMR spectra were acquired with a Varian nuclear magnetic resonance spectrometer at 500 MHz under a standard observation condition [51]. Molecular weights of the dendrimer polymers were measured by matrix assisted laser desorption ionization-time of flight (MALDI TOF) with a Waters TOfsPec-2E spectrometer as described elsewhere [48]. UV-vis absorption spectra were recorded on a Perkin Elmer Lambda 20 spectrophotometer. Purity of the dendrimer conjugate was assessed by the reversed phase analytical UPLC analysis which was carried out on a Waters Acquity Peptide Mapping System equipped with a Waters photodiode array detector [25, 48]. Gel permeation chromatography was performed to determine molecular weights (M_w, M_n) and polydispersity index (PDI = M_w/Mn) of PAMAM G5 dendrimer by using an Alliance Waters 2695 separation module equipped with a Wyatt HELEOS Multi Angle Laser Light Scattering (MALLS) detector, and an Optilab rEX differential refractometer (Wyatt Technology Corporation) [25, 48].

Synthesis of 6 G5-EG (Scheme 1)

To the dendrimer **5** G5-$(GA)_{108}$ (MW = 40,200 g/mol [48]; 1.0 g, 25 μmol) suspended in anhydrous DMF (100 mL) was added *N*-hydroxysuccinimide (NHS, 515 mg), 4-dimethylaminopyridine (DMAP, 546 mg), and then 1-ethyl-3-(3-dimethylaminopropyl) carbodiimide hydrochloride (EDC, 618 mg, 1.2 mol eq to dendrimer glutaric acid). The mixture was stirred at rt for 24 hr. Meantime, the ethylene glycol (EG)-based spacer, $H_2N(CH_2CH_2O)_2CH_2CH_2NHC(=O)(CH_2)_3CO_2H$ (H_2N-EG-GA) was prepared in a separate flask as follows. To the DMF (50 mL) solution containing triethylamine (1.88 mL, 13.5 mmol) was added 3,6-dioxaoctane-1,8-diamine (H_2N-EG-NH_2; 1.0 g, 6.7 mmol), and then glutaric anhydride (0.785 g, 6.9 mmol) as the solution in DMF (5 mL). The reaction mixture was stirred for 12 h at rt while a thick oily residue was precipitated. To this H_2N-EG-GA solution was then mixed with the preactivated G5-GA dendrimer solution prepared above at a molar ratio of [H_2N-EG-NH_2]/[G5-GA] ≈ 270. The final reaction mixture was stirred at rt for additional 12 hr prior to the addition of glutaric anhydride (0.4 g) to cap unreacted primary amine molecules left in the reaction mixture. After stirring additionally for 12 hr, the reaction was terminated by adding water (20 mL), and the mixture was

concentrated *in vacuo*. The solution was diluted with 50 mL of PBS (pH 7.4), and loaded into membrane dialysis tubings (MWCO 10 kDa). It was dialyzed against PBS (2 × 4L), and deionized water (3 × 4L) over 3 days. The aqueous content was freeze-dried to afford **6** G5-EG as beige solid (1.23 g). The dendrimer was characterized by standard analytical methods. UPLC analysis: t_r = 8.52 min; purity ≥95 %. ^{1}H NMR (500 MHz, D_2O): **5** 3.7 (s), 3.6 (s), 3.4-3.3 (m), 2.85 (broad s), 2.7 (broad s), 2.45 (broad s), 2.25 (m), 1.85 (m) ppm where s refers to singlet. GPC: M_w =81450 gmol^{-1}; Mn = 70000 gmol^{-1}; PDI = 1.163. Average number (n = 97) of EG-GA branches present in the dendrimer G5-(EG)n was estimated by the NMR integration method where CH_2 signals (δ 1.8 ppm) in preexisting GA residues (n = 108) were compared to CH_2O signals (δ 3.7–3.8 ppm) in newly attached EG residues.

7 MTX-EG-NH_2

Preparation of **7** was performed in an one-pot process adapted from the amide coupling method of FA with ethylenediamine [62]. To a solution of methotrexate hydrate (24 mg, 51 μmol) in anhydrous DMF (2 mL) was added was added HOBt (7.8 mg, 51 μmol), DIPEA (18 μL, 10 μmol), and then PyBOP (29 mg, 56 μmol). The mixture was stirred for 2 h at rt, and then 3,6-dioxaoctane-1,8-diamine (7.5 μL, 51 μmol) was added to the mixture. The final mixture was stirred for 4 h, and used for *in situ* conjugation with the dendrimer without further treatment. MS (ESI): *m/z* (relative intensity, %) = 567.3 (40) $[M\text{-}NH_3]^+$.

Representative synthesis of G5-(S2)-MTX_n 4 (n = 12)

To the dendrimer **6** G5-$(EG)_{97}$ (100 mg, 1.3 μmol) suspended in anhydrous DMF (10 mL) was added *N*,*N*-diisopropylethylamine (DIPEA; 0.07 mL, 0.4 mmol), HOBt (31 mg, 0.2 mmol), and PyBOP (104 mg, 0.2 mmol). The mixture was stirred at rt for 24 hr prior to the mixing with **7** (51 μmol) dissolved in DMF (2 mL) as prepared above at a molar ratio of [**7**]/[**6**] ≈ 39. The final reaction mixture was stirred at rt overnight, and concentrated *in vacuo*. The crude dendrimer solution was diluted with 10 mL of PBS (pH 7.4), loaded into a membrane dialysis tubing (MWCO 10 kDa), and dialyzed against PBS (2 × 4L), and deionized water (3 × 4L) over 3 days. Free-drying of the aqueous content afforded **4** G5-(S2)-MTX_{12} as pale yellow fluffy solid (101 mg). The dendrimer was characterized by standard analytical methods. UPLC analysis: t_r = 8.73 min; purity ≥98 %. MALDI TOF mass spectrometry: *m/z* = 81300 gmol^{-1}. UV/vis (PBS, pH 7.4): 380, 312, 260 nm. 1H NMR (500 MHz, D_2O): **5** 8.7–8.6 (br), 8.5–8.2 (br), 8.1 (s), 7.8–7.4 (br, m), 6.9–6.8 (br), 6.7–6.4 (br, m), 6.3–6.2 (br), 3.7–3.6 (two s), 3.5–3.2 (m), 2.9–2.8 (br s), 2.7 (s), 2.5–2.3 (br s), 2.3–2.2 (br s), 1.9 (br s) ppm. The number (n ≈ 12) of MTX covalently attached to the dendrimer was estimated on a mean basis by ^{1}H NMR integration method. It compares the value of CH_2 signals (δ 1.8 ppm) in the preexisting GA residues (n = 108) relative to the value of each aromatic proton signal in MTX residues attached [25].

Other analogous conjugate **3** G5-(S2)-MTX_4 was prepared in a similar manner otherwise using a lower molar ratio of [**7**]/[**6**] while adjusting the amounts of other reagents accordingly. UPLC analysis: t_r = 8.68 min; purity 98 %. MALDI TOF mass spectrometry: *m/z* = 79000 gmol^{-1}. UV/vis (PBS, pH 7.4): 380, 312, 260 nm. Another conjugate **2** was prepared in the similar method except that **5** G5-GA[48] replaced **6** G5-EG as the dendrimer. UPLC analysis: t_r = 9.85 min; purity 99 %. UV/vis (PBS, pH 7.4): 380, 310, 260 nm. MALDI TOF mass spectrometry: *m/z* = 46000 gmol^{-1}.

Fluorescent labeling of 4 G5-(S2)-MTX_{12} with Alexa Fluor 488

To a mixture of G5-(S2)-MTX_{12} **4** (15 mg, 0.19 μmol) and HOBt (2 mg, 13 μmol) in anhydrous DMF (5 mL) was added *N*,*N*-diisopropylethylamine (14 μL, 80 μmol), and PyBOP (7.0 mg, 13 μmol). After stirring for 20 min, Alexa Fluor 488 hydrazide (18.7 μmol,

1.4 μmol) dissolved in 1 mL of DMF was added to the reaction mixture. The mixture was stirred overnight at rt, and concentrated *in vacuo*. The residue was dissolved in with 2 mL of PBS solution (pH 7.4), and dialyzed in a membrane dialysis tubing (MWCO 10 kDa) against PBS, and deionized water in the dark. Freeze-drying of the dialyzed solution afforded G5-(S2)-MTX_{12}-AF_3 as pale red fluffy solid (12 mg). Its purity was assessed by analytical UPLC analysis: t_r = 8.84 min; purity ≥98 %. UV/vis (PBS, pH 7.4): 510, 375, 310, 260 nm. The number (n = 3) of Alexa Fluor dye molecules covalently attached to dendrimer was determined on a mean basis by the UV-vis spectroscopy. This method is based on quantitative analysis of its absorption at 494 nm to a standard calibration value prepared by AF 488.

Surface plasmon resonance (SPR) spectroscopy

SPR experiments were run in Biacore® X (Pharmacia Biosensor AB, Uppsala, Sweden). Folate binding protein (FBP, bovine milk) was immobilized onto a CM5 biosensor chip (flow cell 1) coated with a carboxymethylated dextran layer on the gold surface following a standard amide coupling protocol [26, 42–43]. The protein immobilization process resulted in 11000 response unit (RU) equivalent to 11 ng FBP/mm^2. SPR sensorgrams for FBP binding were acquired by injection of each dendrimer or the ligand molecule dissolved in HBS-EP buffer at a flow rate of 20 μL/min (FA, MTX) or 30 μL/min (dendrimers). After each run, the surface of the chip was fully regenerated by injection of 10 μL of 10 mM glycine-HCl (pH 2.5). For the analysis of binding kinetics, a pair of sensorgrams from flow cell 1 (FBP immobilized) and flow cell 2 (reference surface without protein immobilized) was processed to subtract the contribution from non-specific adsorption: $\Delta RU = RU_1$ (flow cell 1) – RU_2 (flow cell 2). Kinetic binding parameters, k_{on} and k_{off}, were extracted by fitting each binding curve separately using non-linear regression analysis as described [57]. The dissociation constant ($K_D = k_{off} \div k_{on}$) determined for each dendrimer conjugate refers to a mean value obtained from multiple independent measurements as specified in the Table 3.

Dihydrofolate reductase (DHFR) assay

The DHFR assay was performed using a kit from Sigma according to the protocol provided, and in a UV-compatible 96-well plate format [43]. Typically, the assay was initiated by adding recombinant human DHFR (1.1 μg/mL) diluted in the assay buffer to a mixture of NADPH (60 μM) and dihydrofolate (DHF; 50 μM) which were premixed with MTX or its conjugate at a variable concentration. The kinetics of the DHF reduction was monitored by following NADPH conversion to NADP by spectrophotometry at 340 nm. Enzyme activity was assessed as reduction rate which was determined from the slope of the linear fitting at the initial phase of reaction kinetics (0–5 min).

Cell Culture

The cells were cultured as a monolayer in FA-deficient RPMI 1640 medium supplemented with 10% fetal bovine serum (FBS). The 10% FBS still contains FA at the concentration equivalent to the human serum concentration (~20 nM). The FR-negative B16-F10 cells were grown in DMEM medium under otherwise similar conditions. All the cells were cultured at 37 °C and under 5% CO_2 atmosphere in the presence of 100 U/ml penicillin, and 100 mg/ml streptomycin.

Flow cytometry

Flow cytometric experiments and analysis were performed as previously described [44, 63]. Cells were plated in 24-well plates and treated with the dye labeled conjugate at different concentrations at 37°C and for 2 hr as specified in Figure 7. Competitive displacement

experiments with FA were performed by pre-incubating with free FA (50 uM) for 30 min prior to the incubation with the conjugate (Figure 8). Then the cells were washed to remove unbound conjugate molecules, and the fluorescence intensity was quantified by using an Accuri flow cytometer (BD Accuri Cytometers, Ann Arbor, MI). The mean FL1-fluorescence of 10,000 cells was determined on a population gated for viable cells. The data were analyzed according to the Accuri software.

In vitro cytotoxicity assay

Cells were seeded in a 96-well microtiter plate (3000 cells/well) in the medium containing dialyzed serum. Two days after plating, the cells were treated with MTX or its dendrimer conjugate in the tissue culture medium for the time period as indicated in Figure 9. A colorimetric assay based on XTT (sodium 3-[1-(phenylaminocarbonyl)-3,4-tetrazolium]-bis(4-methoxy-6-nitro) benzene sulfonic acid hydrate) assay [64] (Roche Molecular Biochemicals, Indianapolis, IN) was performed following the vendor's protocol. After incubation with the XTT labeling mixture, each microtiter plate was read on an ELISA reader (Synergy HT, BioTek) for absorption at 492 nm with the reference value at 690 nm [31].

Acknowledgments

This work was supported by the National Cancer Institute, National Institutes of Health under award 1 R01 CA119409. The author (SKC) thanks Undergraduate Research Opportunity Program (UROP) at University of Michigan for its support, and also for the UROP fellowship (JS). We thank Mr. Ankur Desai for his help in the UPLC and GPC analysis.

References

1. Kukowska-Latallo JF, Candido KA, Cao Z, Nigavekar SS, Majoros IJ, Thomas TP, Balogh LP, Khan MK, Baker JR Jr. Nanoparticle Targeting of Anticancer Drug Improves Therapeutic Response in Animal Model of Human Epithelial Cancer. Cancer Res. 2005; 65:5317–5324. [PubMed: 15958579]
2. Low PS, Henne WA, Doorneweerd DD. Discovery and Development of Folic-Acid-Based Receptor Targeting for Imaging and Therapy of Cancer and Inflammatory Diseases. Acc. Chem. Res. 2008; 41:120–129. [PubMed: 17655275]
3. Majoros IJ, Williams CR, Becker A, Baker JR Jr. Methotrexate Delivery *via* Folate Targeted Dendrimer-Based Nanotherapeutic Platform. WIREs: Nanomed. Nanobiotech. 2009; 1:502–10.
4. Thomas TP, Goonewardena SN, Majoros IJ, Kotlyar A, Cao Z, Leroueil PR, Baker JR. Folate-Targeted Nanoparticles Show Efficacy in the Treatment of Inflammatory Arthritis. Arthritis Rheum. 2011; 63:2671–2680. [PubMed: 21618461]
5. Thomas TP, Choi SK, Li M-H, Kotlyar A, Baker JR Jr. Design of Riboflavin-Presenting PAMAM Dendrimers as a New Nanoplatform for Cancer-Targeted Delivery. Bioorg. Med. Chem. Lett. 2010; 20:5191–5194. [PubMed: 20659800]
6. Thomas TP, Shukla R, Kotlyar A, Liang B, Ye JY, Norris TB, Baker JR Jr. Dendrimer-Epidermal Growth Factor Conjugate Displays Superagonist Activity. Biomacromolecules. 2008; 9:603–609. [PubMed: 18193839]
7. Burkhart DJ, Kalet BT, Coleman MP, Post GC, Koch TH. Doxorubicin-formaldehyde conjugates targeting $\alpha_v\beta_3$ integrin. Mol. Cancer Ther. 2004; 3:1593–1604. [PubMed: 15634653]
8. Farokhzad OC, Cheng J, Teply BA, Sherifi I, Jon S, Kantoff PW, Richie JP, Langer R. Targeted nanoparticle-aptamer bioconjugates for cancer chemotherapy in vivo. Proc. Natl. Acad. Sci. U.S.A. 2006; 103:6315–6320. [PubMed: 16606824]
9. Mullen DG, Desai AM, Waddell JN, Cheng X-m, Kelly CV, McNerny DQ, Majoros InJ, Baker JR Jr, Sander LM, Orr BG, Banaszak Holl MM. The Implications of Stochastic Synthesis for the Conjugation of Functional Groups to Nanoparticles. Bioconjugate Chem. 2008; 19:1748–1752.

10. Majoros IJ, Thomas TP, Mehta CB, Baker JR Jr. Poly(amidoamine) Dendrimer-Based Multifunctional Engineered Nanodevice for Cancer Therapy. J. Med. Chem. 2005; 48:5892–5899. [PubMed: 16161993]
11. Lu Y, Low PS. Folate-mediated delivery of macromolecular anticancer therapeutic agents. Adv. Drug Del. Rev. 2002; 54:675–693.
12. Mullen D, Borgmeier E, Desai A, van Dongen M, Barash M, Cheng Xm, Baker JR Jr, Banaszak Holl M. Isolation and Characterization of Dendrimer with Precise Numbers of Functional Groups. Chem.Eur. J. 2010; 16:10675–10678. [PubMed: 20683917]
13. Hakem IF, Leech AM, Johnson JD, Donahue SJ, Walker JP, Bockstaller MR. Understanding Ligand Distributions in Modified Particle and Particlelike Systems. J. Am. Chem. Soc. 2010; 132:16593–16598. [PubMed: 20977216]
14. Hilgenbrink AR, Low PS. Folate receptor-mediated drug targeting: From therapeutics to diagnostics. J. Pharm. Sci. 2005; 94:2135–2146. [PubMed: 16136558]
15. Thomas, TP.; Kukowska-Latallo, JR. Biological application of PAMAM dendrimer nanodevices in vitro and in vivo. In: Majoros, I.; Baker, JR., Jr, editors. Dendrimer-Based Nanomedicine. Hackensack, NJ: Pan Stanford; 2008. p. 175-207.
16. Li X, Zhou H, Yang L, Du G, Pai-Panandiker AS, Huang X, Yan B. Enhancement of cell recognition in vitro by dual-ligand cancer targeting gold nanoparticles. Biomaterials. 2011; 32:2540–2545. [PubMed: 21232787]
17. Zhou H, Jiao P, Yang L, Li X, Yan B. Enhancing Cell Recognition by Scrutinizing Cell Surfaces with a Nanoparticle Array. J. Am. Chem. Soc. 2010; 133:680–682. [PubMed: 21182273]
18. Montet X, Funovics M, Montet-Abou K, Weissleder R, Josephson L. Multivalent Effects of RGD Peptides Obtained by Nanoparticle Display. J. Med. Chem. 2006; 49:6087–6093. [PubMed: 17004722]
19. Shukla R, Thomas TP, Peters J, Kotlyar A, Myc A, Baker JR Jr. Tumor angiogenic vasculature targeting with PAMAM dendrimer-RGD conjugates. Chem. Commun. 2005:5739–5741.
20. Temming K, Lacombe M, Schaapveld RQJ, Orfi L, Kéri G, Poelstra K, Molema G, Kok Robbert J. Rational Design of RGD-Albumin Conjugates for Targeted Delivery of the VEGF-R Kinase Inhibitor PTK787 to Angiogenic Endothelium. ChemMedChem. 2006; 1:1200–1203. [PubMed: 16991175]
21. Kim Y-H, Jeon J, Hong SH, Rhim W-K, Lee Y-S, Youn H, Chung J-K, Lee MC, Lee DS, Kang KW, Nam J-M. Tumor Targeting and Imaging Using Cyclic RGD-PEGylated Gold Nanoparticle Probes with Directly Conjugated Iodine-125. Small. 2011; 7:2052–2060. [PubMed: 21688390]
22. Lin R-Y, Dayananda K, Chen T-J, Chen C-Y, Liu G-C, Lin K-L, Wang Y-M. Targeted RGD nanoparticles for highly sensitive in vivo integrin receptor imaging. Contrast Media Mol. Imaging. 2012; 7:7–18. [PubMed: 22344875]
23. Hrkach J, Von Hoff D, Ali MM, Andrianova E, Auer J, Campbell T, De Witt D, Figa M, Figueiredo M, Horhota A, Low S, McDonnell K, Peeke E, Retnarajan B, Sabnis A, Schnipper E, Song JJ, Song YH, Summa J, Tompsett D, Troiano G, Van Geen Hoven T, Wright J, LoRusso P, Kantoff PW, Bander NH, Sweeney C, Farokhzad OC, Langer R, Zale S. Preclinical Development and Clinical Translation of a PSMA-Targeted Docetaxel Nanoparticle with a Differentiated Pharmacological Profile. Sci. Transl. Med. 2012; 4:128ra39.
24. Chen Y, Foss CA, Byun Y, Nimmagadda S, Pullambhatla M, Fox JJ, Castanares M, Lupold SE, Babich JW, Mease RC, Pomper MG. Radiohalogenated Prostate-Specific Membrane Antigen (PSMA)-Based Ureas as Imaging Agents for Prostate Cancer. J. Med. Chem. 2008; 51:7933–7943. [PubMed: 19053825]
25. Witte AB, Timmer CM, Gam JJ, Choi SK, Banaszak Holl MM, Orr BG, Baker JR, Sinniah K. Biophysical Characterization of a Riboflavin-conjugated Dendrimer Platform for Targeted Drug Delivery. Biomacromolecules. 2012; 13:507–516. [PubMed: 22191428]
26. Plantinga A, Witte A, Li M-H, Harmon A, Choi SK, Banaszak Holl MM, Orr BG, Baker JR Jr, Sinniah K. Bioanalytical Screening of Riboflavin Antagonists for Targeted Drug Delivery—A Thermodynamic and Kinetic Study. ACS Med. Chem. Lett. 2011; 2:363–367. [PubMed: 21686082]

27. Shukla R, Thomas TP, Desai AM, Kotlyar A, Park SJ, Baker JR Jr. HER2 specific delivery of methotrexate by dendrimer conjugated anti-HER2 mAb. Nanotechnology. 2008; 19:295102. [PubMed: 20686639]
28. Raha S, Paunesku T, Woloschak G. Peptide-mediated cancer targeting of nanoconjugates. WIREs: Nanomed. Nanobiotech. 2010:269–281.
29. Low PS, Kularatne SA. Folate-targeted therapeutic and imaging agents for cancer. Curr. Opin. Chem. Biol. 2009; 13:1–7. [PubMed: 19272831]
30. Kamen BA, Capdevila A. Receptor-mediated folate accumulation is regulated by the cellular folate content. Proc. Natl. Acad. Sci. USA. 1986; 83:5983–5987. [PubMed: 3461471]
31. Thomas TP, Majoros IJ, Kotlyar A, Kukowska-Latallo JF, Bielinska A, Myc A, Baker JR Jr. Targeting and Inhibition of Cell Growth by an Engineered Dendritic Nanodevice. J. Med. Chem. 2005; 48:3729–3735. [PubMed: 15916424]
32. Majoros IJ, Williams CR, Baker J Jr. Current Dendrimer Applications in Cancer Diagnosis and Therapy. Curr. Top. Med. Chem. 2008; 8:1165–1179. [PubMed: 18855703]
33. Ercikan-Abali EA, Waltham MC, Dicker AP, Schweitzer BI, Gritsman H, Banerjee D, Bertino JR. Variants of human dihydrofolate reductase with substitutions at leucine-22: effect on catalytic and inhibitor binding properties. Mol. Pharmacol. 1996; 49:430–437. [PubMed: 8643082]
34. Nandini-Kishore SG, Frazier WA. [^{3}H]Methotrexate as a ligand for the folate receptor of *Dictyostelium discoideum* . Proc. Natl. Acad. Sci. U.S.A. 1981; 78:7299–7303. [PubMed: 6278468]
35. Rijnboutt S, Jansen G, Posthuma G, Hynes JB, Schornagel JH, Strous GJ. Endocytosis of GPI-linked Membrane Folate Receptor-a. J. Cell Biol. 1996; 132:35–47. [PubMed: 8567728]
36. Verwei M, van den Berg H, Havenaar R, Groten JP. Effect of folate-binding protein on intestinal transport of folic acid and 5-methyltetrahydrofolate across Caco-2 cells. Eur. J. Nutr. 2005; 44:242–249. [PubMed: 15316828]
37. Sierra EE, Brigle KE, Spinella MJ, Goldman ID. pH Dependence of methotrexate transport by the reduced folate carrier and the folate receptor in L1210 leukemia cells: Further evidence for a third route mediated at low pH. Biochem. Pharmacol. 1997; 53:223–231. [PubMed: 9037255]
38. Lee YC, Lee RT. Carbohydrate-Protein Interactions: Basis of Glycobiology. Acc. Chem. Res. 1995; 28:321–327.
39. Mammen M, Choi SK, Whitesides GM. Polyvalent Interactions in Biological Systems: Implications for Design and Use of Multivalent Ligands and Inhibitors. Angew. Chem. Int. Ed. 1998; 37:2754–2794.
40. Kiessling LL, Gestwicki JE, Strong LE. Synthetic Multivalent Ligands in the Exploration of Cell-Surface Interactions. Curr. Opin. Chem. Biol. 2000; 4:696–703. [PubMed: 11102876]
41. Roy R. Syntheses and Some Applications of Chemically Defined Multivalent Glycoconjugates. Curr. Opin. Struct. Biol. 1996; 6:692–702. [PubMed: 8913693]
42. Hong, S.; Leroueil, PR.; Majoros, IJ.; Orr, BG.; Baker, JR., Jr; Banaszak Holl, MM. Chem. Biol. Vol. 14. Cambridge, MA, U.S.: 2007. The Binding Avidity of a Nanoparticle-Based Multivalent Targeted Drug Delivery Platform; p. 107-115.
43. Li M-H, Choi SK, Thomas TP, Desai A, Lee K-H, Kotlyar A, Banaszak Holl MM, Baker JR Jr. Dendrimer-Based Multivalent Methotrexates As Dual Acting Nanoconjugates for Cancer Cell Targeting. Eur. J. Med. Chem. 2012; 47:560–572. [PubMed: 22142685]
44. Thomas TP, Huang B, Choi SK, Silpe JE, Kotlyar A, Desai AM, Gam J, Joice M Jr. Polyvalent PAMAM-Methotrexate Dendrimer as a Folate Receptor-Targeted Therapeutic. Mol. Pharmaceutics. 2012; 9:2669–2676.
45. Huang B, Desai A, Zong H, Tang S, Leroueil P, Baker JR Jr. Copper-free click conjugation of methotrexate to a PAMAM dendrimer platform. Tetrahedron Lett. 2011; 52:1411–1414. [PubMed: 21383864]
46. Cody V, Luft JR, Pangborn W. Understanding the role of Leu22 variants in methotrexate resistance: comparison of wild-type and Leu22Arg variant mouse and human dihydrofolate reductase ternary crystal complexes with methotrexate and NADPH. Acta Crystallogr. D Biol. Crystallogr. 2005; 61(Pt 2):147–155. [PubMed: 15681865]

47. Wu G, Barth RF, Yang W, Kawabata S, Zhang L, Green-Church K. Targeted delivery of methotrexate to epidermal growth factor receptor-positive brain tumors by means of cetuximab (IMC-C225) dendrimer bioconjugates. Mol. Cancer Ther. 2006; 5:52–59. [PubMed: 16432162]
48. Choi, SK.; Thomas, T.; Li, M.; Kotlyar, A.; Desai, A.; Baker, JR, Jr. Chem. Commun. Vol. 46. Cambridge, U.K.: 2010. Light-Controlled Release of Caged Doxorubicin from Folate Receptor-Targeting PAMAM Dendrimer Nanoconjugate; p. 2632-2634.
49. Choi SK, Verma M, Silpe J, Moody RE, Tang K, Hanson JJ, Baker JR Jr. A photochemical approach for controlled drug release in targeted drug delivery. Bioorg. Med. Chem. 2012; 20:1281–1290. [PubMed: 22225916]
50. Choi SK, Thomas TP, Li M-H, Desai A, Kotlyar A, Baker JR. Photochemical release of methotrexate from folate receptor-targeting PAMAM dendrimer nanoconjugate. Photochem. Photobiol. Sci. 2012; 11:653–660. [PubMed: 22234658]
51. Choi SK, Leroueil P, Li M-H, Desai A, Zong H, Van Der Spek AFL, Baker JR Jr. Specificity and Negative Cooperativity in Dendrimer-Oxime Drug Complexation. Macromolecules. 2011; 44:4026–4029.
52. Choi SK, Thomas TP, Leroueil PR, Kotlyar A, Van Der Spek AFL, Baker JR. Specific and Cooperative Interactions between Oximes and PAMAM Dendrimers as Demonstrated by 1H NMR Study. J. Phys. Chem. B. 2012; 116:10387–10397.
53. Metallo SJ, Kane RS, Holmlin RE, Whitesides GM. Using Bifunctional Polymers Presenting Vancomycin and Fluorescein Groups To Direct Anti-Fluorescein Antibodies to Self-Assembled Monolayers Presenting d-Alanine-d-Alanine Groups. J. Am. Chem. Soc. 2003; 125:4534–4540. [PubMed: 12683824]
54. Arranz-Plaza E, Tracy AS, Siriwardena A, Pierce JM, Boons GJ. Low-Affinity Multivalent Interactions and the Block to Polyspermy in Xenopus Laevis. J. Am. Chem. Soc. 2002; 124:13035–13046. [PubMed: 12405830]
55. Adler P, Wood SJ, Lee YC, Lee RT, Petri WA Jr. Schnaar RL. High Affinity Binding of the Entamoeba Histolytica Lectin to Polyvalent N-Acetylgalactosaminides. J. Biol. Chem. 1995; 270:5164–5171. [PubMed: 7890626]
56. Mullen DG, Fang M, Desai A, Baker JR Jr, Orr BG, Banaszak Holl MM. A Quantitative Assessment of Nanoparticle-Ligand Distributions: Implications for Targeted Drug and Imaging Delivery in Dendrimer Conjugates. ACS Nano. 2010; 4:657–670. [PubMed: 20131876]
57. Ober RJ, Caves J, Sally Ward E. Analysis of Exponential Data Using a Noniterative Technique: Application to Surface Plasmon Experiments. Anal. Biochem. 2003; 312:57–65. [PubMed: 12479835]
58. Matthews DA, Alden RA, Bolin JT, Filman DJ, Freer ST, Hamlin R, Hol WG, Kisliuk RL, Pastore EJ, Plante LT, Xuong N, Kraut J. Dihydrofolate reductase from Lactobacillus casei. X-ray structure of the enzyme methotrexate.NADPH complex. J. Biol. Chem. 1978; 253:6946–6954. [PubMed: 29045]
59. Lee RJ, Wang S, Low PS. Measurement of endosome pH following folate receptor-mediated endocytosis. Biochim. Biophys. Acta (BBA) - Mol. Cell Res. 1996:237–242.
60. Westerhof GR, Rijnboutt S, Schornagel JH, Pinedo HM, Peters GJ, Jansen G. Functional Activity of the Reduced Folate Carrier in KB, MA104, and IGROV-I Cells Expressing Folate-binding Protein. Cancer Res. 1995; 55:3795–3802. [PubMed: 7641196]
61. Heijden JWVD, Oerlemans R, Dijkmans BAC, Qi H, Laken CJVD, Lems WF, Jackman AL, Kraan MC, Tak PP, Ratnam M, Jansen G. Folate receptor beta as a potential delivery route for novel folate antagonists to macrophages in the synovial tissue of rheumatoid arthritis patients. Arthritis Rheum. 2009; 60:12–21. [PubMed: 19116913]
62. Whiteley JM, Henderson GB, Russell A, Singh P, Zevely EM. The isolation of dihydrofolate reductases by affinity chromatography on folate-Sepharose. Anal. Biochem. 1977; 79:42–51. [PubMed: 405885]
63. Zhang Y, Thomas TP, Desai A, Zong H, Leroueil PR, Majoros IJ, Baker JR. Targeted Dendrimeric Anticancer Prodrug: A Methotrexate-Folic Acid-Poly(amidoamine) Conjugate and a Novel, Rapid, “One Pot” Synthetic Approach. Bioconj. Chem. 2010; 21:489–495.

64. Roehm NW, Rodgers GH, Hatfield SM, Glasebrook AL. An Improved Colorimetric Assay for Cell Proliferation and Viability Utilizing the Tetrazolium Salt XTT. J. Immunol. Methods. 1991; 142:257–265. [PubMed: 1919029]

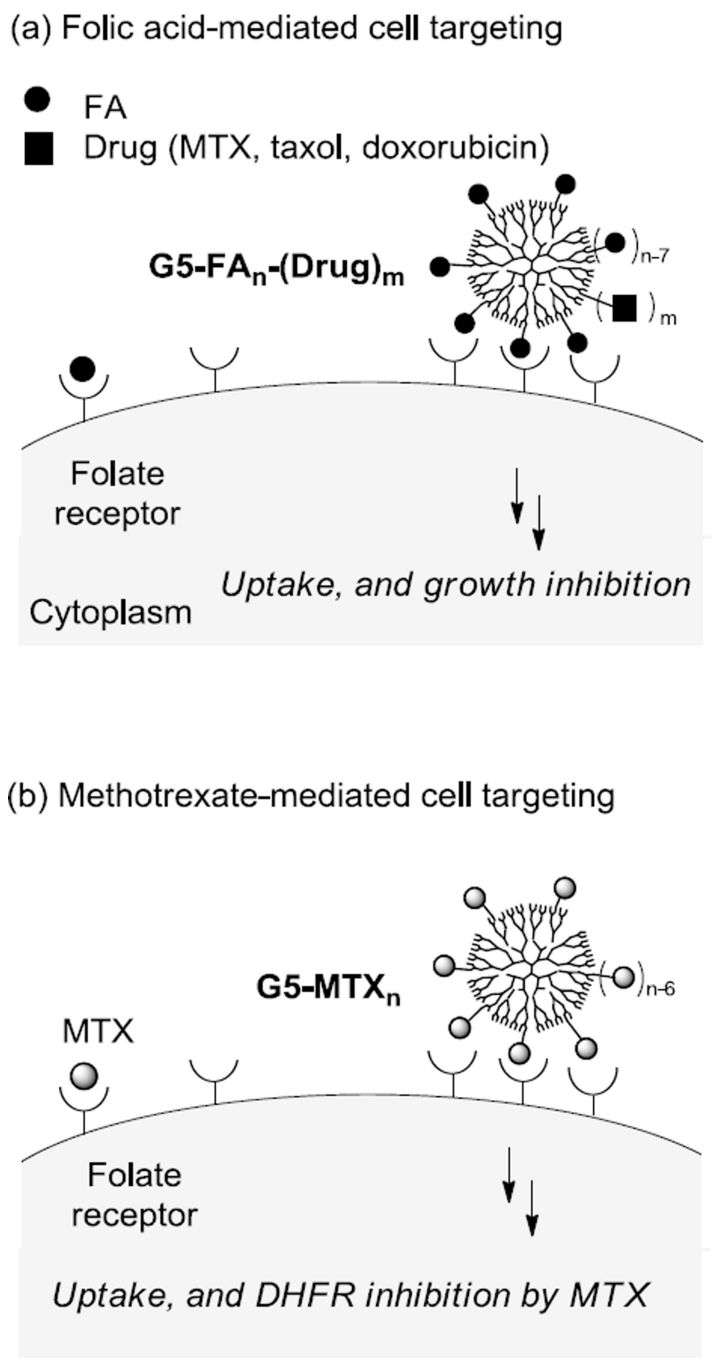

Figure 1.

(a) Schematic for the folic acid receptor (FAR)-targeted drug delivery by a PAMAM dendrimer conjugate G5-FA_n-$(Drug)_m$. The conjugate presents a multivalent array of FA as a targeting ligand and carries cytotoxic drug molecules as payloads including methotrexate (MTX), paclitaxel, and doxorubicin; (b) Schematic for the FAR-targeted MTX delivery by a dendrimer conjugate G5-MTX_n where MTX plays the dual-acting role as a targeting ligand as well as a cytotoxic agent. The figure is not drawn to scale.

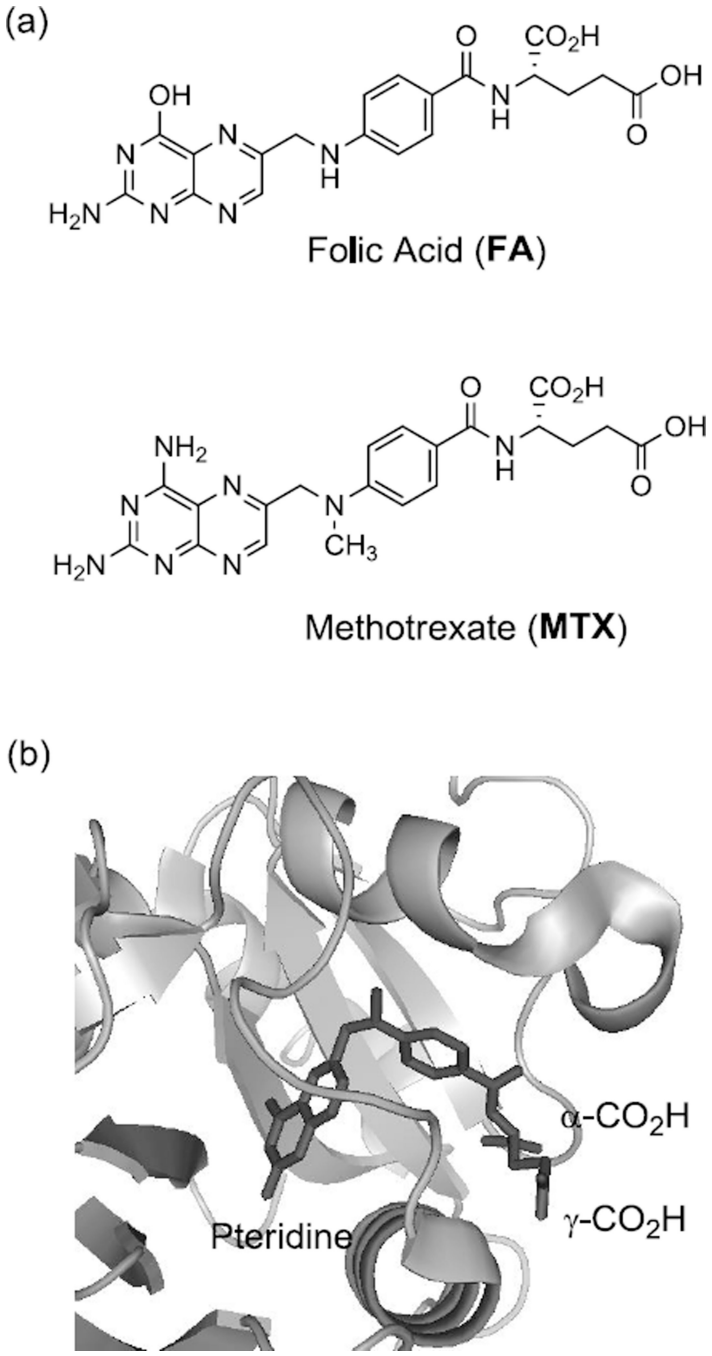

Figure 2.

(a) Structure of folic acid (FA), and methotrexate (MTX); (b) A crystal structure of a methotrexate molecule in complex with human dihydrofolate reductase (hDHFR) at its active site (PDB code 1u72 [46]). Please note that the two carboxylic acids (α, γ) of the MTX L-glutamate residue are exposed out near the entrance to the catalytic pocket, while a pteridine group is bound deep in the pocket. The structural image of the enzyme-inhibitor complex was generated by PyMOL™ (version 1.3).

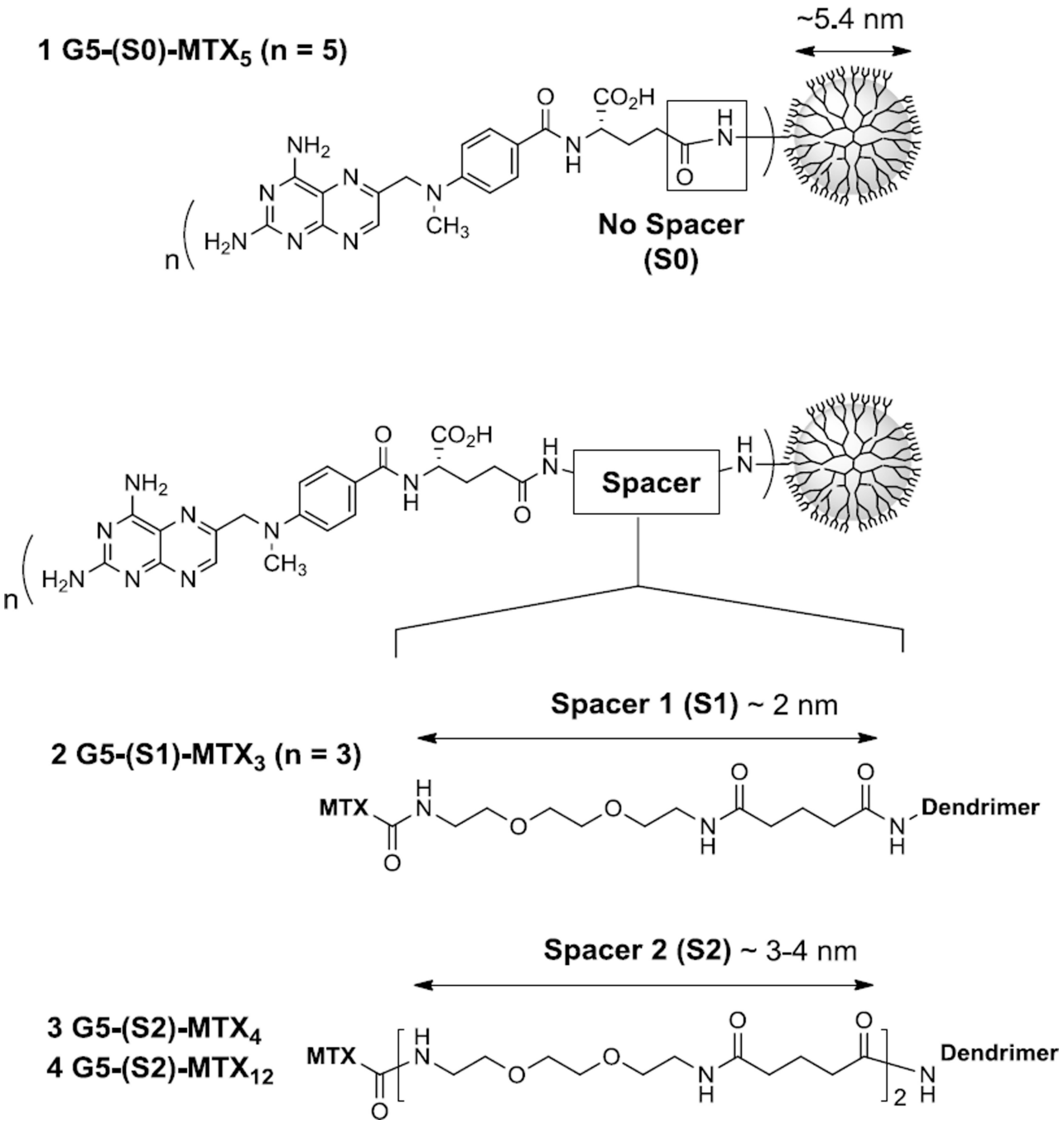

Figure 3.

Structures of methotrexate (MTX)-conjugated dendrimers **1**–**4**. Each conjugate is derived from a fifth generation (G5) PAMAM dendrimer, and presents multiple copies of MTX, each tethered by an amide linkage but through the spacer of variable length as illustrated by no spacer (**1**), spacer 1 (**2**), and spacer 2 (**3,4**). The spacer 1 (S1) is made of one glutaryl-diethyleneglycol unit, while the spacer 2 (S2) is made of two such units (S2 = 2 × S1). Length of each spacer refers to a theoretical value calculated at either a fully extended conformation or a minimized energy conformation (for details, see Table 2). Excess

functional groups that cover the surface of each dendrimer conjugate are not shown for clarity, but include NHAc (**1**), and CO_2H (**2** to **4**).

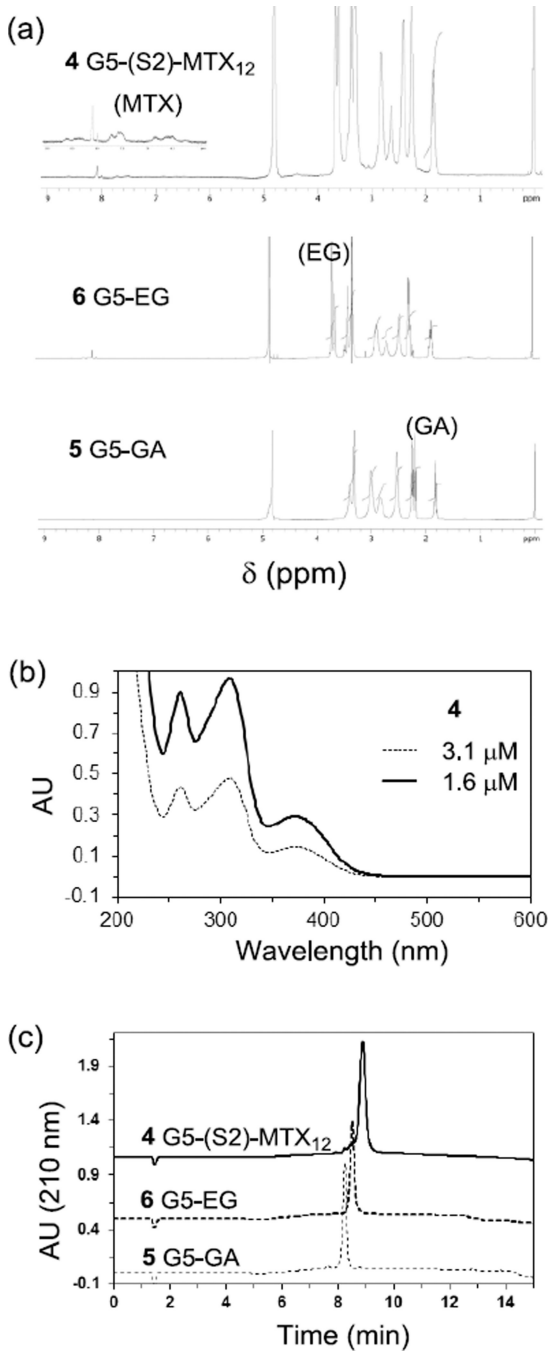

Figure 4.

(a) ^{1}H NMR spectra of **5** G5-GA, **6** G5-EG, **4** G5-(S2)-MTX_{12}; (b) UV/vis spectra of **4** G5-(S2)-MTX_{12}, each measured at 1.6, and 3.2 μM concentration in PBS (pH 7.4); (c) An array of UPLC traces, each for **5** G5-GA, **6** G5-EG, and **4** G5-(S2)-MTX_{12}.

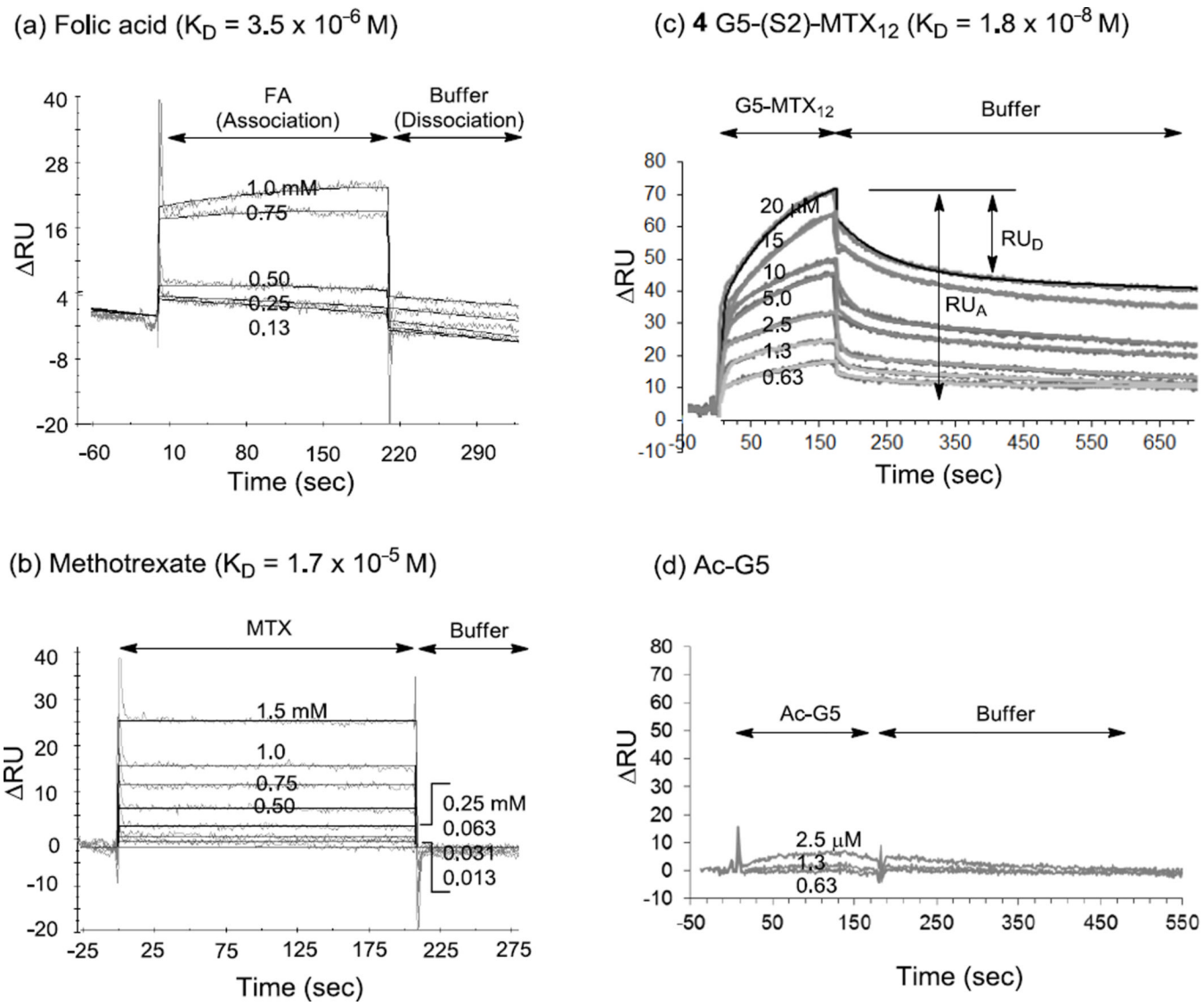

Figure 5.

Surface plasmon resonance (SPR) experiments measuring the binding (association, and dissociation) kinetics of FA, MTX, and dendrimers to bovine folate binding protein (bFBP) immobilized to the surface of a CM5 biosensor chip. (a, b) SPR sensorgrams for monovalent ligands FA, and MTX, respectively, each injected at low mM to high μM concentrations as indicated. (c) SPR sensorgrams for **4** G5-(S2)-MTX_{12}, injected at a range of low μM concentrations. Fractional desorption (= $RU_D \div RU_A$) is defined as the response unit of desorption (RU_D) relative to the total adsorption (RU_A), and varies as a function of time. (d) SPR sensorgrams for Ac-G5, the dendrimer tested as a negative control which has no MTX tethered.

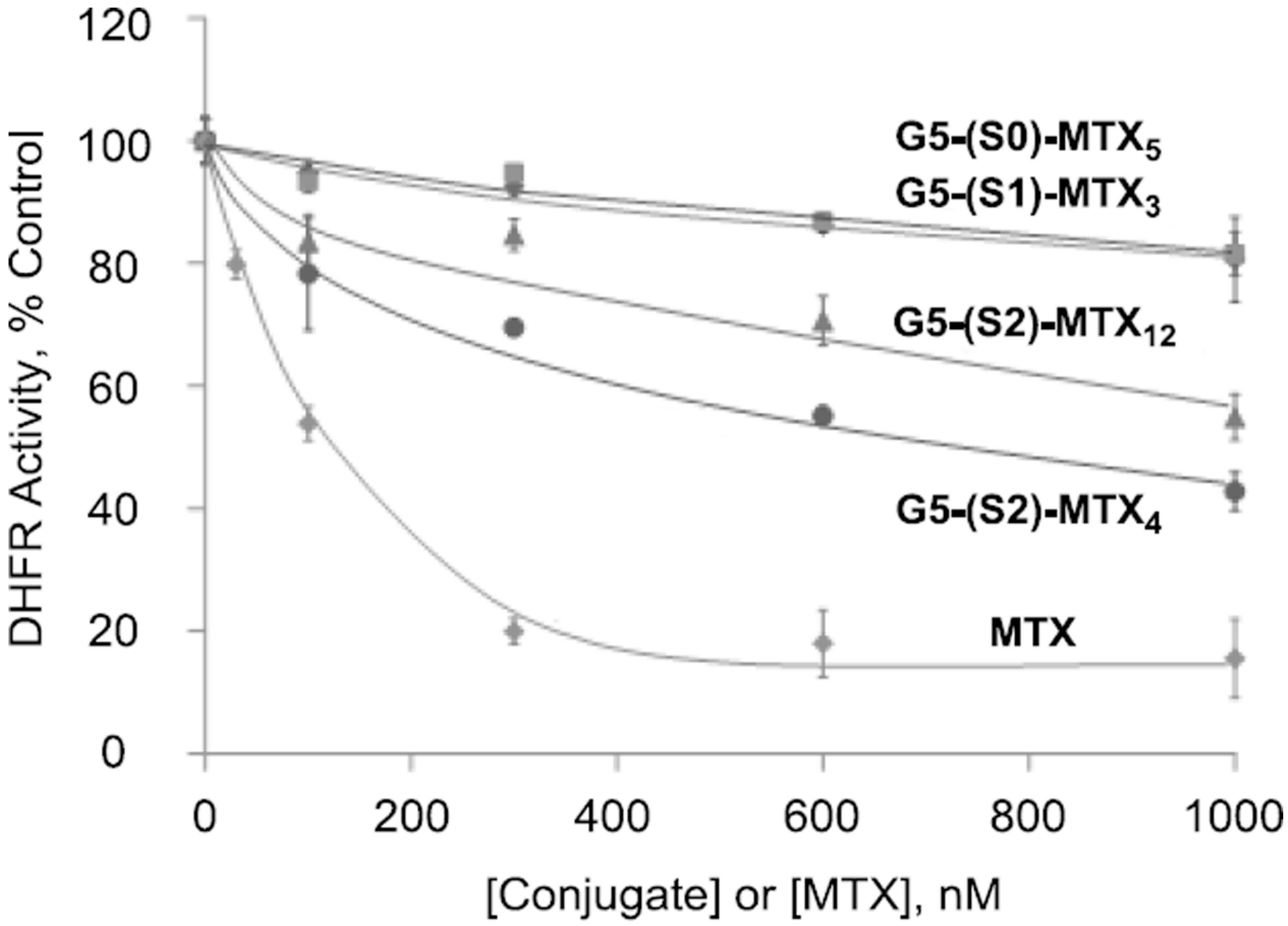

Figure 6.

Dose-dependent inhibition of recombinant DHFR by G5-MTX_n conjugates and MTX. The inhibition of DHFR activity by different concentrations of G5-MTX_n or MTX was determined as described in Methods. The enzyme activity is expressed as percent controls obtained in the absence of the drug or conjugates. G5-MTX_n conjugates: G5-(S0)-MTX_5 (**1**), G5-(S1)-MTX_3 (**2**), G5-(S2)-MTX_4 (**3**), G5-(S2)-MTX_{12} (**4**). Each data point represents a Mean ± SE of three different experiments.

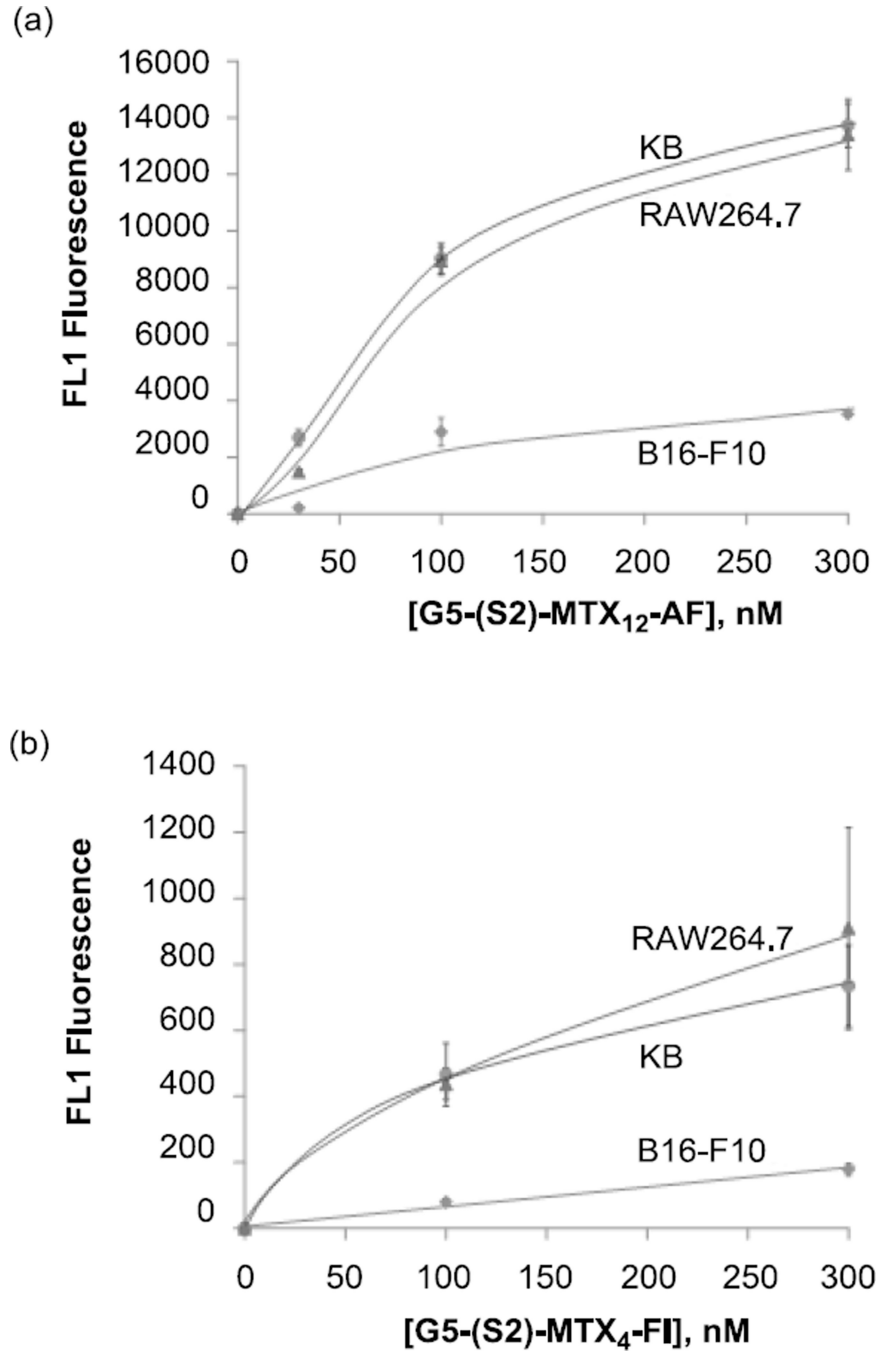

Figure 7.

Binding of G5-(S2)-MTX_{12}-AF_3 (a) and G5-(S2)-MTX_4-FI_2 (b) in the high FAR-expressing KB and RAW264.7, and in the low FAR-expressing B16-F10 cells. Cells were treated with each conjugate for 2 hr and rinsed, and the mean fluorescence of gated live cells was quantified as given in Methods. The data represent background-subtracted Mean ± SE of multiple cell samples from 2–5 independent experiments, each obtained by acquiring the mean fluorescence of 10,000 cells. Abbreviations for fluorescent dyes: AF = Alexa fluor 488; FI = fluorescein isothiocyanate (FITC).

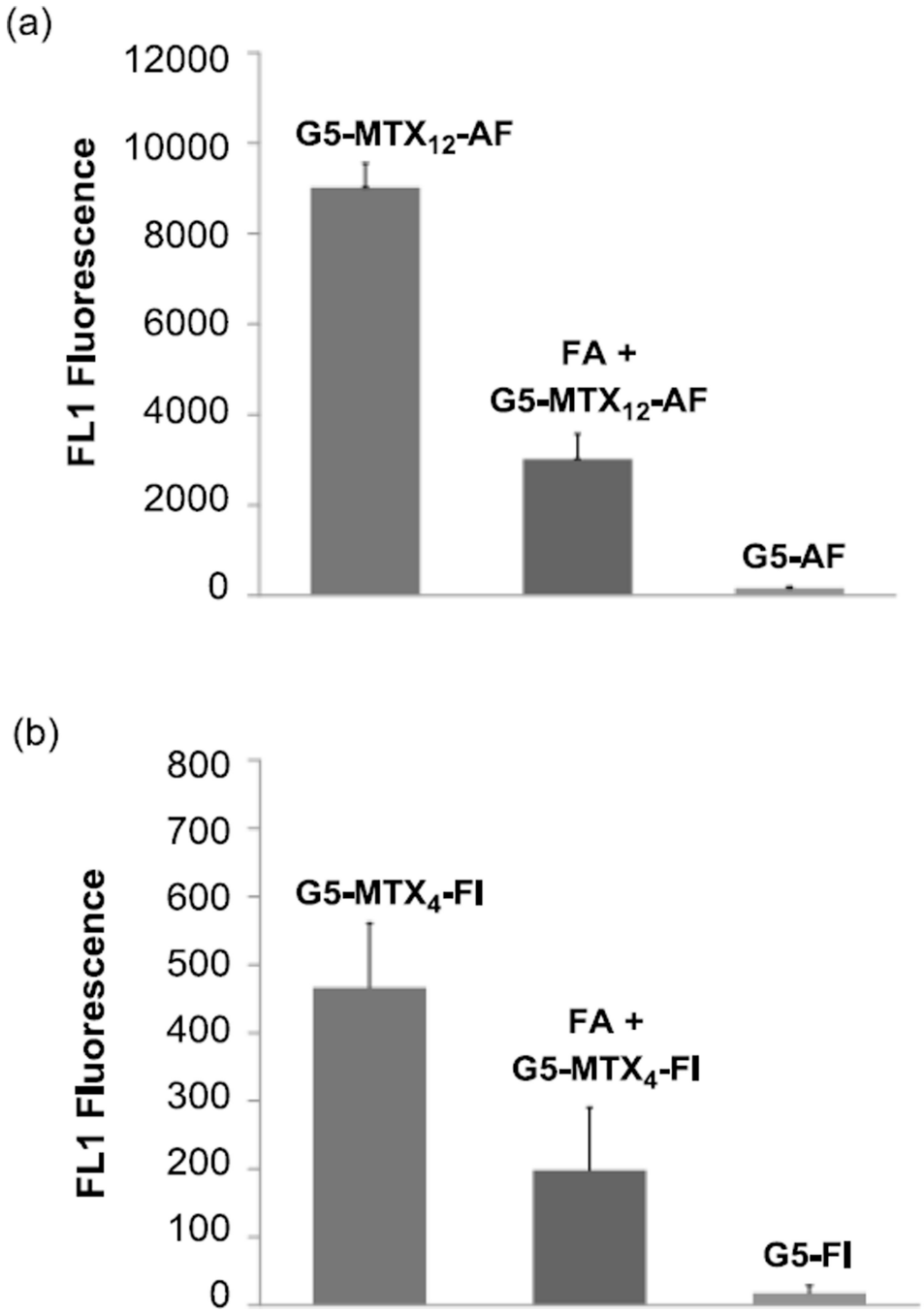

Figure 8.

Demonstration of FAR-specificity of G5-(S2)-MTX_{12}-AF_3 (a) and G5-(S2)-MTX_4-FI_2 (b) for binding to FAR-expressing KB cells. Cells were incubated with 100 nM of each MTX-conjugate and its respective control conjugate (G5-AF or G5-FI) that lacks MTX for 2 hr, and the FL1 fluorescence was determined as given in Methods. Some cells were also pre-incubated with 5 μM free FA for 30 min prior to incubation with 100 nM of the targeted conjugate (middle panels). To correct the difference in the mean number of fluorescent dye molecules attached to each conjugate particle such as G5-(S2)-MTX_{12}-AF vs. G5-AF control, the fluorescence intensity was normalized by measuring the fluorescence of standard solutions of the conjugates in a spectrofluorimeter. The height of each bar

represents a background-subtracted Mean ± SE fluorescence of 3 – 4 cell samples, each derived from the analysis of 10,000 cells.

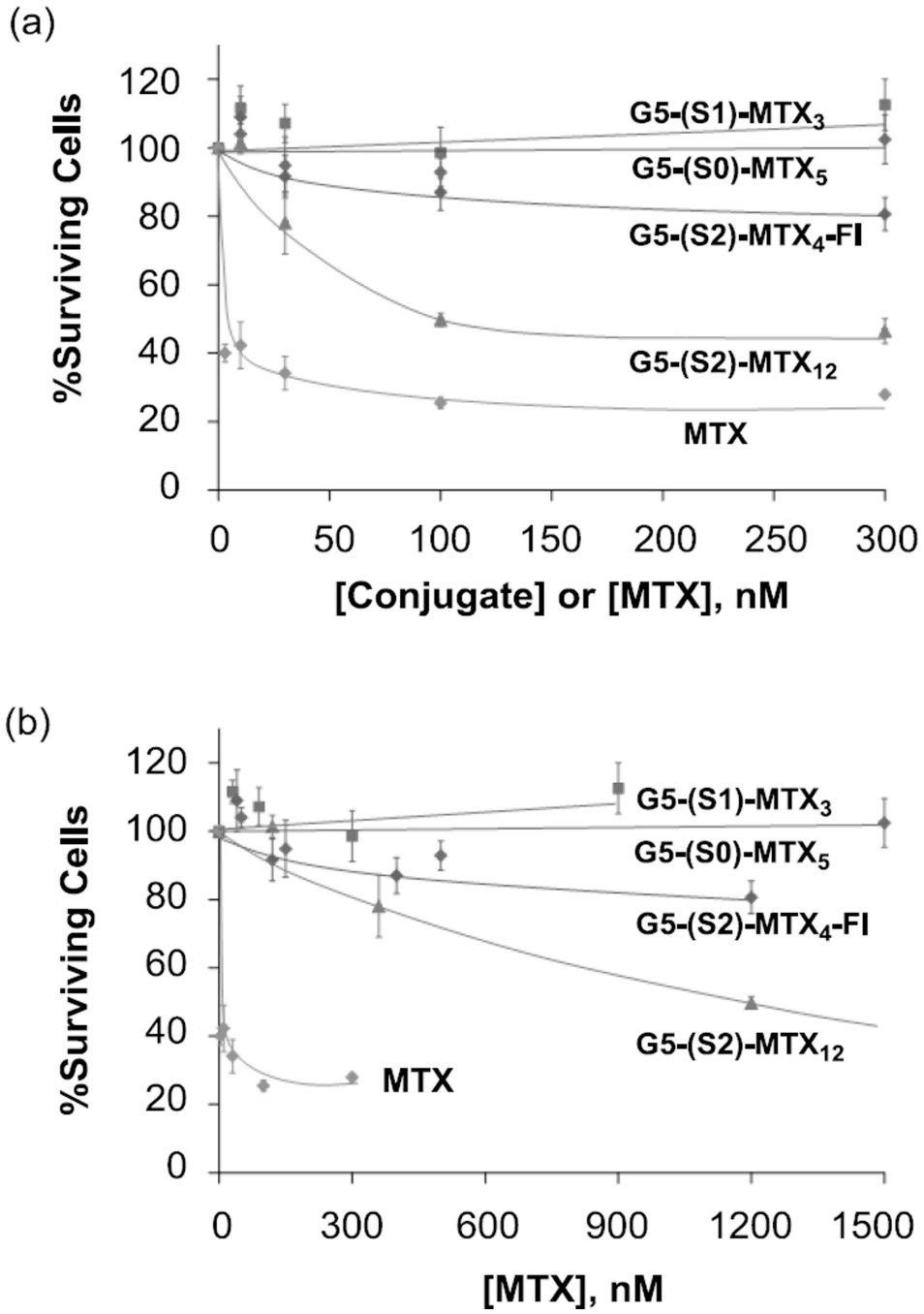

Figure 9.

Cytotoxicity of G5-MTX_n conjugates in KB cells. Cells were incubated for 3 days with the indicated conjugates or free MTX, and the cytotoxicity was determined by XTT assay as given in Methods. The data represent the Mean ± SE of 8–12 cell samples from two independent experiments. The X-axis values for each conjugate are expressed as conjugate-based (a) or MTX-based (b) concentrations.

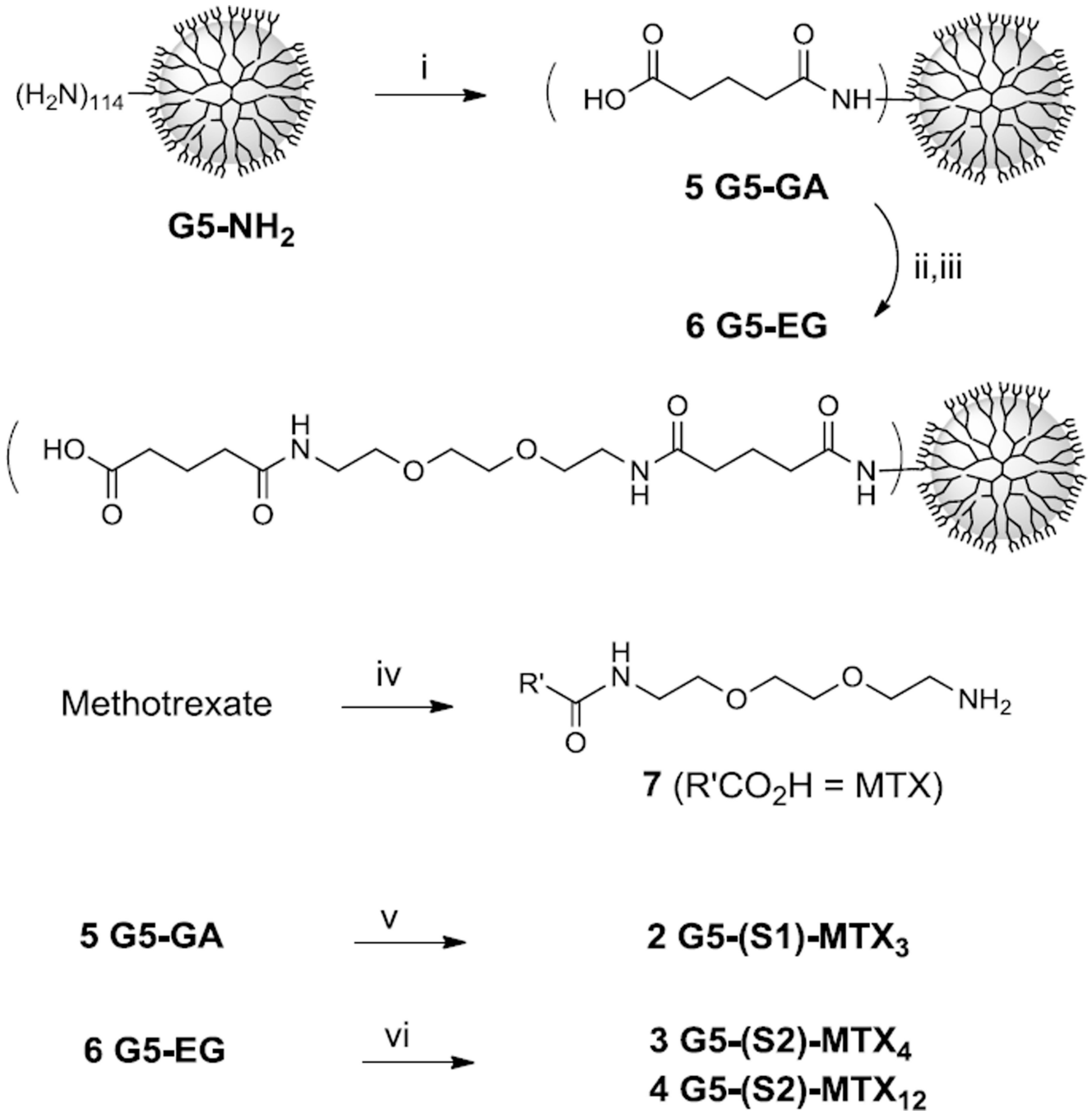

Scheme 1.

Synthesis of MTX-conjugated G5 PAMAM dendrimers **2–4**, each MTX molecule tethered to the dendrimer through an EG-based spacer. *Reagents and conditions*: i) Glutaric anhydride, Et_3N, MeOH, rt; ii) EDC, NHS, DMAP, DMF, rt; iii) $H_2N(CH_2CH_2O)_2CH_2CH_2NHC(=O)(CH_2)_3CO_2H$, Et_3N, rt, DMF; iv) (a) PyBOP, HOBt, DIPEA, DMF; (b) $H_2N(CH_2CH_2O)_2CH_2CH_2NH_2$; v) (a) EDC, NHS, DMAP, DMF, rt; (b) **7**, Et_3N, rt; vi) (a) PyBOP, HOBt, DIPEA, DMF; (b) **7**, rt.

Table 1

Pharmacological activities and physicochemical properties of folic acid (FA) and methotrexate (MTX)

	MW (g/mol)	*a*,*b*LogD (pH 7.0)	Caco2 permeability [36] (×10^{-6} cm/sec)	*b*,*c*tPSA (Å^2)	K_D (FAR)	K_i (DHFR)	Trophic Activity
FA	441.4	−5.82	1.7	208	0.4 nM[30]	-	Positive
MTX	454.4	−4.98	1.2	211	20–100 nM[30, 34–35]	1.2 nM[33]	Negative

*a*D = distribution coefficient = $[Drug]_{octanol} \div [Drug]_{buffer}$

*b*Calculated using Advanced Chemistry Development (ACD/Labs) Software V11.02

*c*tPSA = total polar surface area

Table 2

Selected molecular and physicochemical properties of Spacer 1 and 2

	[a]No. of Atoms	[b]Length (Å)	[c]Length (Å)	[d,e]LogP	[e,f]tPSA (Å^2)
Spacer 1 (S1)	15	22	16	−2.33	106
Spacer 2 (S2)	30	44	27	−3.93	184

[a]Counted between the MTX carboxyl (carbon) and the terminal nitrogen of G5 dendrimer

[b]Calculated at a fully extended conformation (ChemDraw 3D)

[c]Calculated at a minimized energy conformation (MM2)

[d]LogP = log([Spacer]$_{octanol}$ ÷ [Spacer]$_{water}$); P = partition coefficient; calculated as an amide form at each terminus of the spacer

[e]Calculated using Advanced Chemistry Development (ACD/Labs) Software V11.02

[f]tPSA = total polar surface area

Table 3

Rate constants and equilibrium dissociation constants K_D for the binding of folic acid (FA), methotrexate (MTX), **1** G5-(S0)-MTX_5 [43], and **4** G5-(S2)-MTX_{12} to the folate binding protein (FBP) immobilized on the surface of a CM5 biosensor chip as determined by surface plasmon resonance (SPR) spectroscopy.

	k_{on} ($M^{-1}s^{-1}$)	k_{off} (s^{-1})	$^{a}K_D$ (M)	$^{b}\beta$
FA	-	-	3.5×10^{-6}	-
MTX	-	-	1.7×10^{-5}	1
1	$^{d}3.4\ (\pm2.5)\times10^{4}$	$^{d}8.7\ (\pm2.5)\times10^{-4}$	$^{d}2.6\ (\pm1.0)\times10^{-8}$	923 (185^{c})
4	1.3×10^{5}	$5.9\ (\pm3.1)\times10^{-4}$	$1.8\ (\pm1.7)\times10^{-8}$	944 (79^{c})

[a] Dissociation constant K_D (= $k_{off} \div k_{on}$) represents a mean value calculated by averaging the data obtained from seven different injection concentrations, each duplicated per concentration. The number within parentheses refers to the standard error of the mean (SEM), and unless noted specifically, the standard error for the K_D or k_{on} value is within 2-fold variation.

[b] β = Multivalent binding enhancement = $K_D^{MTX} \div K_D^{G5\text{-}MTX}$

[c] The value within parentheses refers to the valency (n)-corrected value (= $\beta \div n$) where n = 5 (conjugate **1**) or n = 12 (conjugate **4**).

[d] Data cited [43]